PHILOSOPHICAL TRANSACTIONS OF THE ROYAL SOCIETY A

Phil. Trans. R. Soc. A (2011) **369**, 4255–4277
doi:10.1098/rsta.2011.0129

Pulmonary embolism: predicting disease severity

By K. S. Burrowes[1,*], A. R. Clark[2], A. Marcinkowski[2], M. L. Wilsher[4], D. G. Milne[3] and M. H. Tawhai[2]

[1]*Department of Computer Science, University of Oxford, Wolfson Building, Parks Road, Oxford, OX1 3QD, UK*
[2]*Auckland Bioengineering Institute, and* [3]*Anatomy with Radiology, University of Auckland, Private Bag 92019, Auckland 1142, New Zealand*
[4]*Respiratory Services, Auckland District Health Board, Private Bag 92024, Auckland, New Zealand*

Pulmonary embolism (PE) is the most common cause of acute pulmonary hypertension, yet it is commonly undiagnosed, with risk of death if not recognized promptly and managed accordingly. Patients typically present with hypoxemia and hypocapnia, although the presentation varies greatly, being confounded by co-mordidities such as pre-existing cardio-respiratory disease. Previous studies have demonstrated variable patient outcomes in spite of similar extent and distribution of pulmonary vascular occlusion, but the pathophysiological determinants of outcome remain unclear. Computational models enable exact control over many of the compounding factors leading to functional outcomes and therefore provide a useful tool to understand and assess these mechanisms. We review the current state of pulmonary blood flow models. We present a pilot study within 10 patients presenting with acute PE, where patient-derived vascular occlusions are imposed onto an existing model of the pulmonary circulation enabling predictions of resultant haemodynamics after embolus occlusion. Results show that mechanical obstruction alone is not sufficient to cause pulmonary arterial hypertension, even when up to 65 per cent of lung tissue is occluded. Blood flow is found to preferentially redistribute to the gravitationally non-dependent regions. The presence of an additional downstream occlusion is found to significantly increase pressures.

Keywords: pulmonary embolism; computational modelling; redistribution of blood flow

1. Introduction

To counteract the neglect of lung health and to raise awareness of the urgency to tackle lung diseases, the Forum of International Respiratory Societies declared 2010 to be 'The Year of the Lung' (www.yearofthelung.org). It is therefore timely to consider the role of predictive computational modelling of the respiratory system, in particular that associated with physiome and virtual physiological

*Author for correspondence (kelly.burrowes@cs.ox.ac.uk)

One contribution of 11 to a Theme Issue 'Towards the virtual physiological human: mathematical and computational case studies'.

human (VPH)-related respiratory projects, which has developed somewhat in the shadows of other organ system modelling, such as cardiac or musculoskeletal. Development towards a lung physiome (www.physiome.org.nz/lung) includes compiling a digital atlas of the human lung for male and female subjects spanning several decades of age [1], deriving computation-ready models of structure to partner the digital atlas [2–5], and implementation of mathematical models to study structure–function relationships and system interactions [6–9]. These efforts are summarized in several review papers [9–11]. The prominence of respiratory disease and increasing morbidity and mortality associated with respiratory illnesses such as chronic obstructive pulmonary disease (COPD; currently rated the fourth biggest killer by the World Health Organization [12]) provide strong motivation for clinically driven model development within this area.

Here, we focus on describing efforts to develop predictive models of lung structure–function for studying redistribution of blood flow and development of pulmonary hypertension (PH) secondary to pulmonary embolism (PE). We present a structure-based analysis of perfusion within the pulmonary vasculature to further our understanding of the integrative mechanisms that impact on gas exchange, as a result of redistribution of blood post-PE. A multi-scale model incorporating the important structural and passive functional features of the pulmonary circulation is used to facilitate analysis of patient-specific data. Morphometrically consistent arterial and venous vessel structures are connected via a model of the microcirculation [13] and both macro- and micro-flow models incorporate the effect of lung tissue deformation owing to gravity. Each of these components of the pulmonary circulation, along with the location and size of the emboli, has an effect on the clinical severity of PE.

PE is a relatively common clinical condition that can result in acute or chronic elevation in pulmonary artery pressure (PAP) inducing secondary PH. If left untreated, chronic elevations in PAP may lead to right ventricular (RV) hypertrophy and ultimately to RV failure (cor pulmonale). PE is difficult to diagnose because of its range of symptoms and clinical features; however, the capability to stratify risk among PE patients is vital to enable optimal management [14]. PE elevates PAP owing to an increase in pulmonary vascular resistance (PVR), the severity of which is determined by several factors including embolus size, location, population, severity of occlusion, existence of prior cardiopulmonary disease and vasoactive mechanisms. PE is a potentially correctable cause of PH via medical management or surgery. However, most patients with chronic PH secondary to PE present late in the course of the illness; therefore, understanding the mechanism of disease development and predicting progression to RV failure can often be difficult or impossible.

Despite the prevalence of PE, it is still not clear precisely how it affects gas exchange on a patient-specific basis, and how the degree of hypoxemia and elevation of RV pressure varies according to embolus distribution and severity. Here, we focus on understanding how blood flow is redistributed in the presence of pulmonary emboli. We provide an introduction to the disease, and then review previous modelling studies in this area and present new results on the application of an existing anatomically-based, multi-component model of the pulmonary circulation [15] to assess blood flow redistribution during vascular obstruction. Computed tomography pulmonary angiography (CTPA) from 10

patients acquired during routine clinical examination for PE is used to define the location of emboli. Statistical analysis of the patient data showed correlation between RV dysfunction and degree of obstruction, which leads to the central question of this model-based study: to what extent can RV dysfunction in PE be attributed to mechanical obstruction of the vasculature, and can the contribution of signalling from the embolus via vasoactive mediators be quantified? We aim to understand the perfusion in PE at the level of the integrated organ system, and how this contributes to risk for the patient. This provides a clear demonstration of how the 'next generation' of lung physiome/VPH models can be used to address clinically important questions.

2. Pathophysiology of pulmonary embolism

PE is associated with high mortality when not treated and high total treatment cost that is compounded by recurrent PE and secondary disease. PE typically involves some degree of PH, which is defined clinically by a mean PAP greater than 25 mm Hg at rest or greater than 30 mm Hg during exertion [16], in comparison with a normal resting mean PAP from 10–14 mm Hg with an upper limit of normal of approximately 20 mm Hg [17]. Both PE and deep vein thrombosis (DVT) are manifestations of venous thromboembolism (VTE), a condition that is also associated with high morbidity and mortality [18]. PE occurs when a segment of a blood clot detaches and lodges in the pulmonary arteries. Massive PE as a consequence of DVT is one of the most common causes of unexpected natural death, particularly in relatively young people [19,20]. Sub-massive PE is surprisingly prevalent but difficult to diagnose [21] because presenting signs and symptoms are non-specific and screening tests are not always sensitive enough to detect disease in asymptomatic patients. The condition is often overlooked in patients with comorbid disease, and it appears that up to 70 per cent of PE is only detected at autopsy [21–24].

CTPA is frequently used as an initial diagnostic tool for PE [25,26]. CTPA is used to locate large emboli, typically to the level of the segmental arteries. The severity of obstruction can be estimated by calculating obstruction indices (OIs) based on the size and proportion of each artery occluded (such as the Miller, Walsh, Mastora or Qanadli scores [14]). The Walsh score additionally takes into account whether occlusion is in the upper, middle or lower lobes of the lung, with lower lobe occlusions weighted the highest, followed by upper, then middle lobe. There is debate in the literature as to how definitive clot load scores are for assessing patient risk. Medical studies have shown that RV failure, resulting from both the amount of occlusion and any variable additional factors, is a better indicator of the severity of PE than OIs on their own [14]. While this is an intuitive outcome and is a direct measure of patient survivability, it does not provide any quantification or understanding of the variable impacts of RV dysfunction.

PE is also characterized by ventilation/perfusion (V/Q) abnormalities leading to impaired gas exchange, hypoxemia and hypocapnia [27]. Redistribution of both ventilation and perfusion after occlusion plays a deterministic role in these outcomes. In addition to the presence of high V/Q regions caused by vascular obstruction and increased physiological dead space distal to the occlusion, blood flow is redistributed to non-occluded regions producing areas of decreased V/Q

owing to higher than normal blood flow rates. While the broad impact of this is known, exactly how blood is redistributed within non-occluded regions is not well understood.

Embolic PH may be caused by a direct mechanical obstruction of the pulmonary arterial tree, but there is mounting evidence that pulmonary vasoconstriction via the release of vasoactive mediators from platelet thrombi (for example, serotonin and thromboxane A_2) also plays a prominent role in the immediate response to embolus occlusion, elevating its impact on PAP [28–30].

There is considerable variation in disease severity and patient survival post-embolus occlusion, even when patients have apparently similar levels of vascular occlusion [31,32]. Even with diagnosis and treatment, a proportion of patients are at high risk for recurrent PE and the development of chronic PH [33–35] in response to hypoxaemia and increased PVR. Cor pulmonale develops in up to 70 per cent of patients with massive PE [20]. Recurrent PE and secondary disease further increase the high total healthcare costs associated with the condition [36]. The risk of recurrent PE depends in part on the amount of tissue affected and the coexistence of other conditions, and some patients continue to experience VTE despite treatment with anticoagulants [37]. The response to PE is heterogeneous, and predicting which patients will develop acute or chronic PH is difficult [38,39]; the key to preventing PH and repeating PE therefore lies in early diagnosis and treatment. A comprehensive and carefully constructed theoretical model would provide the ability to quantify the contribution of each mechanism contributing to outcomes in PE, by simulating function when each mechanism is active or inactive. The model that is considered in the following section includes only the most important *passive* features of the pulmonary circulation; however, the contribution of *active* features can still be postulated based on the consistency or lack of consistency of predicted function compared with clinical measurements.

3. Current state-of-the-art in modelling of the pulmonary circulation and pulmonary embolism

(*a*) *Models of the pulmonary circulation*

Models of blood flow in the larger pulmonary blood vessels have used either a systems (electrical analogue) approach [40], or a physiological approach that solves flow equations in a more realistic geometry [15,41–44]. Recently, three-dimensional computational fluid dynamics (CFD) has been used to simulate blood flow in anatomically accurate models of pulmonary blood vessels [44]. While this approach includes structural detail and theoretically provides the most accurate prediction of pressure, flow and wall shear stress, it is also computationally expensive and therefore can only realistically be applied to a small portion of the vascular tree, e.g. the proximal three or four arterial generations [44]. It is important to be aware that the level of detail required in a computational model is governed by the question being posed. When it is necessary to consider the distribution of blood throughout the extensive branching network of the entire pulmonary circulation, it also becomes necessary to use a more simplified set of governing equations than those used in three-dimensional CFD, and/or simplified representations of the branching geometry. Highly idealized symmetric [43,45] and self-similar fractal [46] tree models have been useful for investigating

global flow characteristics and for conceptual studies to probe the underlying mechanisms that dictate perfusion distribution; however, they are unable to predict realistic spatial distributions of blood, particularly within the individual patient. To address this limitation, others have used one-dimensional (centreline) models with geometry based on imaging of the *in vivo* lung [47], or with imaging-based geometry supplemented with additional 'virtualized' arteries and veins [3,6,15,42] to model the accompanying pulmonary arterial and venous trees in their entirety. These one-dimensional geometries necessitate the use of one-dimensional governing equations, which are derived from the generalized equations for fluid dynamics by making simplifying assumptions, in particular, that radial and azimuthal flows are negligible. The one-dimensional Poiseuille flow equation, which is used in the current study, assumes laminar, incompressible, steady flow along a tube of uniform cross section. This simplified equation enables predictions of flow throughout a full anatomically based geometric model.

Models of the pulmonary microcirculation fall into two categories: sheet flow and tube flow. The former, established by Fung & Sobin [48], approximates the dense pulmonary capillary bed as a sheet of fluid flowing around posts of connective tissue, and bounded by the compliant capillary wall. This approximation provides an efficient prediction of average blood flow and cellular transit times through an alveolar septum. In contrast, tube flow models depict the capillary bed as a network of discrete tubes (in both the pulmonary [49–51] and systemic [52–54] microcirculations). The latter approach is computationally expensive in comparison with the sheet flow model, and requires detailed information about the capillary network geometry. Once again, the level of model detail depends on the question that is being asked. Here, we are considering emboli that lodge within the pulmonary arteries; the sheet flow model is therefore an appropriate representation of the microcirculation for such a study.

In order to link macro- and micro-circulatory level models, appropriate representation of intra-acinar vessel flow is required. Most models of the full pulmonary vascular circuit have treated intra-acinar vessels in the same manner as the macrocirculation in terms of branching structure and governing physical equations [40,55]. In these models, arterioles and venules are coupled at the most distal location with a microcirculatory unit; that is, the capillary bed is supplied in parallel by the arterioles. However, the *in vivo* intra-acinar vessel structure differs substantially from the large arterial and venous trees owing to vessels that regularly branch off to feed the capillary bed that enwrap the alveolated surface of the acinar airways. This combined series and parallel structure have been termed 'ladder-like' by Clark *et al.* [13]. In this previous study, intra-acinar blood flow was modelled with specific consideration of intra-acinar vessel structure, which was shown to be important for simulating increased blood flow via capillary recruitment.

(*b*) *Models applied to studying alterations during pulmonary embolism*

In a previous modelling study, Mélot *et al.* [56] adopted a simplified Starling resistor model (based on Mitzner & Sylvester [57]) and a distensible vessel model (based on Haworth *et al.* [58] and Zhuang *et al.* [59]) to investigate which model best described the relationship between PAP and flow in embolic PH in dogs. Their simulations provided reasonably accurate predictions of experimentally

derived PAP flow and PAP–LAP (left atrial pressure) curves pre- and post-embolic occlusion. Roselli & Parker [60] also applied a rudimentary model to investigate the effect of embolization on measurement of capillary pressure via venous occlusion. While these models were able to address specific experimentally led questions, they were not designed to provide regionally varying, anatomical information or details of perfusion alterations at the micro-circulatory scale pre- or post-occlusion. Our model, presented in the following section, is somewhat more complex than previous models; however, this is necessary to enable predictions of regional variation in perfusion parameters both at the macro- and micro-scale within the pulmonary vascular circuit that have not previously been possible.

4. Application of an anatomically based computational model to perfusion assessment post-occlusion

Here, we present data from a pilot study in which we applied a structure-based theoretical model that integrates experimental and clinical observations to 10 adult patients with PE, to understand elevated RV pressure and ultimately hypoxaemia as a result of distributions of emboli.

(*a*) *Patient data*

Volumetric CTPAs were acquired from 10 adult subjects undergoing imaging for clinically suspected acute PE at Auckland City Hospital. Subjects underwent pulmonary function testing to confirm that they had otherwise normal lung function. The absence of existing lung disease was confirmed in each subject and embolus locations were determined to the level of segmental arteries by an expert radiologist. A Qanadli obstruction index (QOI) [61] was also calculated for each subject. The QOI is a CT-based index designed to quantify the degree of arterial obstruction based on the number of segmental arteries occluded. The arterial tree of each lung is typically considered to have 10 segmental arteries (three in the upper lobes, two in the middle lobes and the lingula and five in the lower lobes, illustrated in the model in figure 1*a*). To calculate a percentage QOI the following formula can be applied:

$$\sum \frac{(nd)}{40} \times 100\%, \tag{4.1}$$

where n is the number of segmental arteries occluded by the embolus (n is between 1 and 20) and d is the degree of obstruction ($d = 0$, no obstruction; $d = 1$, partial obstruction; $d = 2$, full obstruction). Values for QOI, and the presence or absence of RV dilation and dysfunction are presented in table 1. The mean QOI was 47.0 per cent (s.d. 18.8%). The ratio of mean pulmonary artery (mPA) to aorta diameter is another suggested measure of PH severity obtainable from CT; values are listed in table 1. A ratio of mPA/aorta greater than 1.0 indicates a very high probability of PH [62]. Measurements of oxygen (O_2) saturation are also included

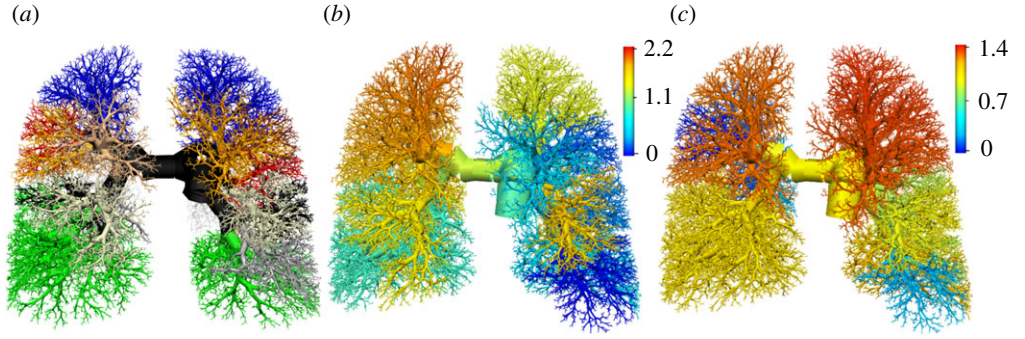

Figure 1. (*a*) The segmental definition in the model (10 pulmonary segments are defined in each of the left and right lungs—this is in accordance with the QOI calculation. The different colours in each lung represent the different segments). (*b*,*c*) The flow redistribution ($Q_{\text{occluded}}/Q_{\text{baseline}}$, these values are represented using the colour range specified by the colour bar in the upper right inset) using the patient-specific occlusion information derived from CTPA for subjects 6 and 9, respectively. In (*b*,*c*), red indicates the highest $Q_{\text{occluded}}/Q_{\text{baseline}}$ and blue the lowest, values are indicated on the colour spectrum.

Table 1. Patient information and percentage QOI (equation (4.1)) for each PE subject.

subject	QOI (%)	RV dilation	RV dysfunction	mPA/aorta	O_2 saturation
1	57.5	yes	yes	0.81	98
2	65	yes	yes	0.98	95
3	25	yes	no	0.95	95
4	45	yes	no	1.19	95
5	55	yes	yes	1.07	98
6	65	yes	yes	1.32	99
7	5	—	—	0.98	94
8	52.5	no	no	1.11	97
9	55	yes	yes	0.93	93
10	45	yes	yes	0.91	97

for each patient in table 1. Statistical analysis of the measurements in this study show a correlation between mPA/aorta and the amount of tissue occluded (QOI, $p = 0.02$).

The QOI for each subject was compared with pulmonary perfusion metrics, heart rate, respiratory rate and systemic blood pressure (as given in table 1) as well as the results of simulations (described below). Correlation between variables was assessed using the Pearson correlation coefficient. Weak correlations were found between the QOI and systemic blood pressure ($p < 0.10$) and a stronger correlation was found between QOI and RV dysfunction ($p < 0.05$). There was no significant correlation between the QOI and percentage oxygen (O_2) saturation in blood. Therefore, in these subjects with acute PE, the QOI appears to be a reasonable indicator of RV dysfunction, which is caused by an increased PVR, and subsequently results in a decrease in systemic blood pressures. However, it is not an indicator of gas exchange abnormalities, which may affect long-term PE outcomes. Model predictions (a description is provided below) of PAP and

Table 2. Analysis of emboli locations from the CTPA patient data summed over all patients and flow partitions (as a percentage of cardiac output (CO)) to the left and right lungs and each of the five lobes as predicted via the flow model. PA, pulmonary artery; RPA, right pulmonary artery; RUL, right upper lobe; RML, right middle lobe; RLL, right lower lobe; LPA, left pulmonary artery; LUL, left upper lobe; LLL, left lower lobe.

location	no. arteries occluded	total occlusions found %	flow partition, upright (% CO)
PA	0	0	—
RPA	4	2.3	51.7
RUL	39	22.8	11.7
RML/RLL	9	5.3	—
RML	15	8.8	9.1
RLL	32	18.7	30.9
LPA	2	1.2	48.3
LUL	30	17.5	17.6
LLL	40	23.4	30.7

PVR correlated with measured QOI ($p = 0.01$ for both PAP and PVR), but did not correlate with RV dilation or dysfunction. This highlights the importance of mechanical obstruction, but indicates the presence of other factors impacting on outcomes.

(*b*) *Distribution of emboli*

Large emboli were found to extend along the length of several vessels; therefore, instead of using the number of emboli to assess the distribution of occlusions, we used the number of arterial vessels occluded. A total of 171 super-segmental vessels were fully or partially occluded by emboli across the 10 patients (mean 17.1 ± 6.8 per subject). More emboli were found in the right lung (57.9%) compared with the left (42.1%). There was a slight preference for emboli lodgement within the lower lobes, particularly in the left lower lobe (23.4%). A high proportion of occlusions were also present in the right upper lobe (22.8%). Full vessel occlusion was only found in approximately 12 per cent of the vessels; emboli were commonly found to saddle bifurcation points and partially occlude downstream branches. These results are listed in table 2. We predicted the percentage of total cardiac output flowing into the left and right lungs and into each of the lobes from the model flow results under normal conditions (with no occlusions). Results (table 2, column 4) demonstrate a slightly higher proportion of flow into the right lung, which may account for the higher probability of emboli in this lung. More flow travels to the lower lobes, again indicating embolus transport is in proportion to flow rates.

Some analysis of embolus distribution in human [63,64] and rabbit lungs [65] has previously been conducted. Oser *et al.* [64] assessed the location of emboli in 76 patients in order to assess the probability of peripheral emboli lodgement, which are more difficult to detect using cross-sectional imaging. They identified a total of 205 emboli, a mean of 2.7 emboli per patient, where the largest arterial branch involved was predominantly segmental (50.7%), followed by subsegmental

(26.7%), lobar (18.7%) or smaller (5%). These were found to be distributed anatomically, with 53 per cent in the right lung (16% in the upper, 9% in the mid and 25% in the lower lobe) and 47 per cent in the left lung (14% in the upper and 26% in the lower lobe). Only 37 per cent of the emboli were found to fully occlude vessels. These occlusions are distributed in a similar proportion to both the patient occlusions from the current study and the flow partitions calculated from the model (table 2).

(*c*) *The baseline computational model*

Specific details of the components of the model used here can be found in [13,15,41,42]. The combination of the separate model components described below into a single integrated model is described in detail in Clark *et al.* [15], and the essential equations are repeated in appendix A. To summarize, this model includes the following features:

- Anatomically based geometry of the lung surface and central blood vessels.
- Computationally generated morphometrically consistent models of the 'accompanying' arterial and venous vessels (i.e. not including supernumerary vessels) to the level of the acini. There are approximately 64 000 each of arterial and venous branches, and each terminal vessel in this model is associated with a single pulmonary acinus (of which there are approximately 32 000 in the whole lung).
- A simplified intra-acinar flow model [13] consisting of nine symmetric branches of intra-acinar arteries and veins coupled in a serial and parallel arrangement through a 'sheet' flow representation of the pulmonary capillaries [66].
- A model of parenchymal tissue deformation [67], to which the vascular networks are tethered. Tissue deformation influences perfusion via shift in the vessel locations (the 'Slinky' effect [68]), elastic recoil pressures acting to distend the extra-capillary vessels, and the effect of alveolar inflation levels on capillary sheet distensibility [15,41].

A prediction of blood flow through the full pulmonary circuit (arteries, capillaries, veins) can be obtained after applying boundary conditions for pressure or flow at the level of the heart. In this study, we are assessing a lung at functional residual capacity (FRC) in the upright posture. We apply an inlet flow of $5\,\mathrm{l\,min^{-1}}$ at the pulmonary trunk (Q_{RV}), and left atrial pressure (LAP) of 5 mm Hg. By solving equations for Poiseuille resistance, conservation of mass, vessel elasticity and a microcirculatory model—including gravity—(further details can be found in appendix A and in Clark *et al.* [15]), predictions can be obtained for the regional distribution of blood, blood and transmural pressures, capillary recruitment and vessel radius. Blood within the larger vessels is assumed to be Newtonian; however, in the microcirculatory vessels, the shear-thinning properties of blood are accounted for via an apparent viscosity parameter in the model equations.

Using this integrated model for the pulmonary circulation—which represents the baseline (no occlusions) model behaviour in the current study—Clark *et al.* [15] showed that each structural and gravitational feature of the pulmonary circulation makes a distinct contribution to the distribution of blood. Early experimental studies suggested that gravity was the primary determinant of

blood flow distribution in the lung, owing to the hydrostatic pressure gradient affecting the balance of forces at the capillary level and hence allowing or limiting flow [69]. The classic description of blood flow distribution is therefore gravitationally dependent, with lung tissue in the non-dependent region (apices of the upright lung) receiving proportionately less of the cardiac output than tissue in the dependent region (base of the upright lung). More recent studies have highlighted irreversibility of the flow gradient with reversal of posture [70], and large iso-gravitational heterogeneity of flow [71], both of which somewhat contradict the gravitational theory for flow distribution. Clark *et al.* [15] showed that postural differences in perfusion gradients can be explained by the combined effect of tissue deformation and extra-acinar blood vessel resistance to flow in the dependent tissue. However, the model also demonstrated that gravitational perfusion gradients persist when the effect of tissue deformation is eliminated, highlighting the importance of the hydrostatic effects of gravity on blood distribution. Heterogeneous large vessel resistance (owing to geometric asymmetry of the vascular trees) was shown to cause variation in driving pressures across the microcirculation. This variation was amplified by the complex balance of pressures, distension and flow at the micro-circulatory level, resulting in relatively large iso-gravitational heterogeneity of tissue perfusion.

(*d*) *The post-occlusion computational model*

For each of the 10 subjects, the percentage of arterial occlusion in each artery from the main pulmonary artery to the level of the segmental arteries was estimated from their CT images, for use in post-occlusion simulations. These percentage occlusions were mapped onto the computational model, and their effect was approximated by reducing the radius of the artery at this location. To achieve this, measurements were made of the diameter of identified emboli and the arteries in which they lie at multiple points along the length of the vessel. The proportion of occlusion within the artery is then calculated as the average of these measured values. Where occlusion levels vary considerably within a vessel, the vessel is represented by multiple finite elements with different levels of occlusion in each element. To predict the haemodynamic consequence of the patient-specific distribution of emboli, the perfusion model was re-solved under baseline boundary conditions ($\mathrm{LAP} = 5\,\mathrm{mmHg}$ and $Q_{\mathrm{RV}} = 5\,\mathrm{l\,min^{-1}}$). That is, the occlusions were assumed not to increase LAP or to decrease Q_{RV}. The effect of degree of occlusion, as reflected by the QOI, on predictions of PAP (after the vascular occlusions were defined within the model for each of the 10 subjects) is illustrated in figure 2. We fitted an exponential curve to this data ($R^2 = 0.85$).

In addition, we imposed (i) vascular constriction, (ii) a reduction in vessel elasticity, and (iii) fixed capillary recruitment in an attempt to investigate the effect of these mechanisms on resultant PAP. The current vascular model does not include generation of active forces within the vascular wall; however, smooth muscle cell contraction, which may occur as a result of vasoactive signalling during embolus occlusion, would result in a reduction of the internal blood vessel radius. Therefore, to investigate the effect of vascular constriction on predicted PAP, we reduced all vessel radii to 80 per cent of their baseline value. To assess the effect of vessel elasticity, the parameter describing vessel distensibility (α, defined in eqn 1 in [15]) was decreased. This single parameter determines how much the

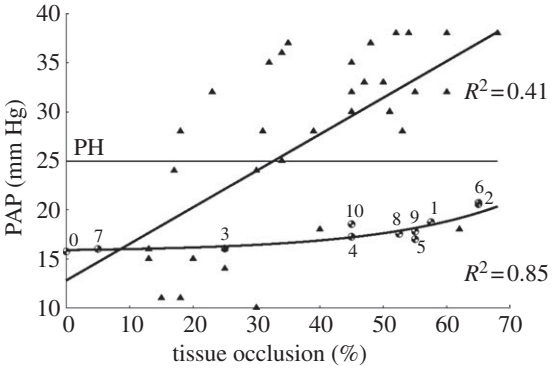

Figure 2. Plot showing the relationship between the volume of tissue occluded (%), as represented by the Qanadli obstruction index (QOI) for the patient data in this study, and the predicted mean pulmonary arterial pressure (PAP, mm Hg). Model predictions for each of the 10 subjects are labelled with their corresponding number, '0' represents the baseline simulation with no occlusions. We fit an exponential curve to the model predictions (half-filled circles, $R^2 = 0.85$). Data from the studies of McIntyre & Sasahara [31,32] (triangles) are included on this plot and display much higher PAPs and a large range of potential PAP outcomes for similar volumes of occluded tissue. The straight line fit is from McIntyre data from both of these studies ($R^2 = 0.41$). Half-filled circles, model; triangles, human data. The horizontal line drawn at PAP = 25 mm Hg is the cut-off for clinically defined pulmonary hypertension (PH).

internal radius of each extra-capillary vessel will expand at a given transmural pressure. Vessel distensibility was decreased by setting α to 80 per cent of the baseline value ($\alpha_b = 1.50 \times 10^{-4}\,\mathrm{Pa}^{-1}$). To assess the effect of recruitment, we removed the capillary recruitment variability by setting capillary recruitment (R) to a fixed value of 70 per cent of capillaries recruited (the average baseline recruitment fraction). After each of these alterations, the simulations were re-run and new values for PAP, PVR and blood flow distributions were obtained. When applied independently, none of these mechanisms were sufficient to increase PAP to hypertensive levels for any volume of occluded tissue in this study. We found that PAP increased twice as much (approx. 14%) as a result of vascular constriction compared with the reduction in vessel elasticity (PAP increased approx. 7%). Setting a fixed capillary recruitment did not significantly change overall PAP, but did result in a reduction of the gravitational flow gradient (because the level of capillary tissue available for perfusion was set constant throughout the lung rather than a function of pressure and therefore gravity—the recruitment model is described in appendix A). Results in figure 3 show the effect of all three mechanisms applied simultaneously.

On figures 2 and 3, we have included measurements from the studies of McIntyre & Sasahara [31,32]. In these studies, haemodynamic data were measured in multiple patients (with no prior cardiopulmonary disease) with variable levels of tissue obstruction. The percentage of tissue occluded was estimated by quantifying the reduction in tissue opacification or radioactivity from pulmonary angiography. While this method applies a slightly different image-based prediction of occlusion, both techniques (this one and QOI scoring used in the patient cohort in this study) aim to estimate the proportion of lung tissue affected by vascular occlusion; therefore, we directly compare PAP values at these

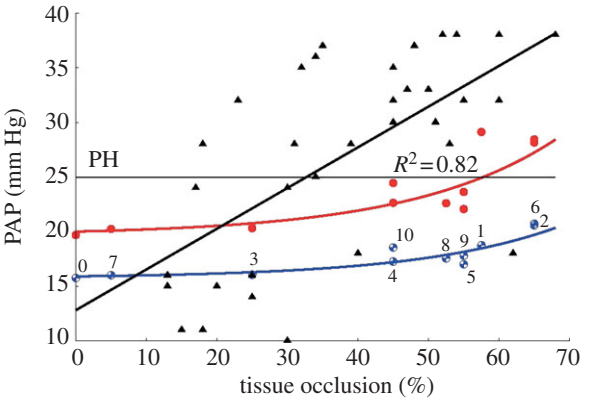

Figure 3. PAP (mm Hg, from model predictions, circles and measured data [32], triangles) plotted with respect to the volume of occluded tissue (%). The blue data (half-filled circles) show model predictions using normal model properties, model (i) [15]. The red data (circles) illustrate model predictions after including: vasoconstriction (radii = 80% of baseline), reduced vessel elasticity (elasticity = 80% of baseline) and uniform capillary recruitment of 70% (the mean value) throughout the lung tissue, model (ii). Model predictions for each of the 10 subjects are labelled with their corresponding number, '0' represents the baseline simulation with no occlusions. The horizontal line drawn at PAP = 25 mm Hg is the cut-off for clinically defined pulmonary hypertension (PH).

measured levels of occlusion in figures 2 and 3. The data showed a reasonably good correlation between PAP and obstruction level; however, a fairly large amount of heterogeneity was evident across subjects. These data showed that most subjects with greater than 30 per cent of tissue occluded had PAP at a hypertensive level (PAP > 25 mm Hg). These data display, on average, much higher PAP values for a given occlusion than those predicted via our simulations. A horizontal line is draw in figures 2 and 3 at PAP = 25 mm Hg to represent the cut-off for clinically defined pulmonary hypertension [16]. All model results in figure 2 are below this line, indicating that a hypertensive level is not reached with mechanical occlusion alone, even with occlusions of up to 65 per cent; this indicates that additional factors must be acting to increase PVR and resultant PAP. Figure 3 shows the possible effect of vasoconstriction, reduced vessel elasticity and uniform capillary recruitment on predicted PAP. The combined effect of these factors is to increase PVR and so to increase predicted PAP.

One potential mechanism contributing to heterogeneity of PAP for a given image-based measurement of tissue obstruction is the presence of small sub-segmental occlusions. This is something that is not able to be assessed clinically (CTPA indices generally only extract occlusion information down to the segmental level) and would be difficult, if not impossible, to assess experimentally. However, through the model, we can readily postulate the impact of additional downstream occlusions on total PVR and resultant increase in PAP. We have conducted preliminary investigations in subject 1 of the patient cohort. Six different vascular locations, located one vessel downstream of a measured segmental occlusion (the first sub-segmental vessels), were occluded by reducing their radius to 10 per cent of its baseline value. PAP was calculated for each additional occlusion, and showed a range of increase from between

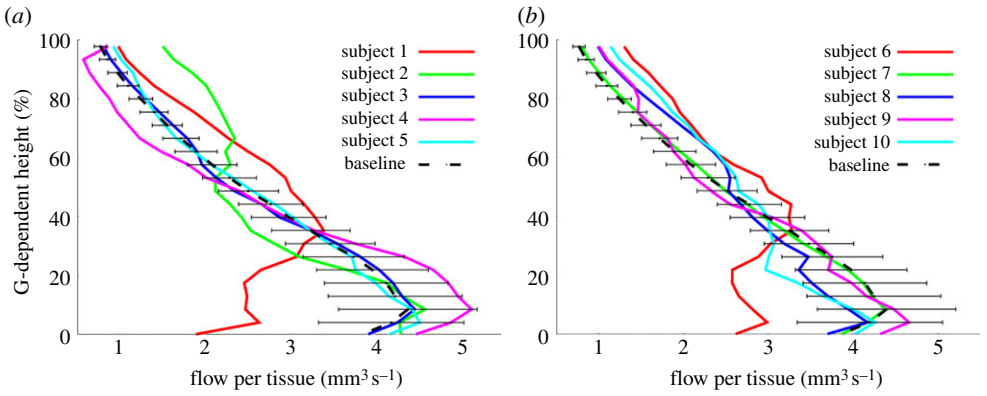

Figure 4. Illustration of the redistribution of pulmonary blood flow post-occlusion in (*a*) patient 1–5 and (*b*) 6–10, both plots include the baseline model blood flow prediction. Blood flow per acinar tissue ($mm^3\,s^{-1}$) is plotted with respect to gravitationally dependent height (%) in the upright model. Acinar flow values are averaged within 10 mm slices. All subject data, excluding subject 4, show an increase of blood flow in the non-dependent regions.

18 and 35 per cent after one additional downstream occlusion (baseline PAP for subject 1 was 18.7 mm Hg; maximal PAP of 35.7 mm Hg = an increase of 35%). This suggests that small unresolved occlusions downstream from an embolus could cause considerable increase in PAP; this is an area that merits further investigation in multiple subjects, particularly in those subjects in whom sub-segmental emboli can be resolved.

(*e*) *Redistribution of blood flow post-occlusion*

Simulations post-embolus occlusion predict preferential redistribution of blood to the gravitationally non-dependent regions. Figure 1*b*,*c* illustrates redistribution of blood flow as the ratio of post-occlusion to baseline flow ($Q_{\text{occluded}}/Q_{\text{baseline}}$), for the patient-specific occlusions present in subjects 6 and 9, respectively. Redistribution to the non-dependent regions is evident, and is also illustrated by figure 4 showing blood flow distribution as a function of gravitationally dependent height. Note that this blood flow distribution is the flow that is delivered to the alveolar tissue, which here is defined as the flow exiting each distal-most pre-acinar arteriole. This is also referred to as the 'flow to the tissue'. Perfusion gradients (calculated as a function of gravitationally dependent height in the lung using linear regression) and coefficient of variation (COV) are calculated for this 'per tissue' flow.

All subjects, excluding subject 4, demonstrated the same pattern of redistribution to non-dependent regions (figure 4). Subject 4 had several occlusions in the upper lung and therefore did not show increased blood flow in these regions. This pattern of redistribution is due to increased potential for capillary recruitment in the upper lung (shown in a previous modelling study [15]) owing to lower baseline capillary pressures and therefore lower recruitment at baseline. This mechanism helps to distribute increased blood flow more evenly within non-occluded regions and also minimizes detrimental effects of high flow such as reduction of red blood cell transit times and increased capillary pressures.

Calculation of COV per isogravitational slice showed that flow heterogeneity increased within lung slices containing vascular occlusion, as would be expected for regions with both depressed and elevated flow.

5. Discussion

This study provides a new understanding of pulmonary perfusion that relates underlying structure to inter-subject variability in function and presentation of symptoms in PE. By improving knowledge in this area, we aim to ultimately understand the range of morbidity in PE from patients with subclinical embolism to those who develop PH. Model results show that, in general, blood redistributes preferentially to non-dependent lung tissue following PE, highlighting the importance of embolus location as a predictor of PE severity. We show that mechanical obstruction alone (to the segmental level) is insufficient to increase PAP to a hypertensive level, even with 65 per cent of tissue occluded (figure 3), supporting the hypothesis that vasoactive signalling is an important contributor to PE outcomes. The model further shows that if sub-segmental vessels are occluded in addition to partial occlusion of larger vessels (for example, owing to the break-off of part of a large embolus), increases in PVR can be significant.

CTPA provides valuable structural information, but the relationship between the anatomical picture and the physiological mechanisms leading to RV failure and mortality is not fully understood. This relationship cannot be adequately studied using clinical data owing to lack of resolution of CTPA and an inability to test 'what if' scenarios. Computational models enable exact control over many of the compounding factors leading to functional outcomes and therefore will provide a useful tool to understand and assess these mechanisms. At least part of the variable response to PE treatment is due to heterogeneity in embolus location. A structure-based model for PE is therefore essential to capture regionally varying changes in the distribution of perfusion post-occlusion. This type of model should be able to replicate observable perfusion measures; for example, it should compare well with measured PVR and distributions of perfusion observed via imaging. In addition, modelling can provide information on the effect of embolization at spatial scales that cannot be easily captured in routine CTPA, or on properties of pulmonary perfusion that are invasive to measure. Computational models can isolate each factor contributing to disease outcome, and quantify their potential impact on disease severity. This mechanistic insight ultimately has the potential to be used to guide diagnostic procedures and improve patient outcomes.

(*a*) *Redistribution of blood flow*

Hypoxemia in PE is largely a result of impaired V/Q matching [27,72,73]. Under normal conditions, there is a gravitationally dependent gradient of V/Q, both in animals [74] and in humans [75], whereby V/Q decreases from (>1) in non-dependent to (<1) in dependent regions. Altemeier *et al.* [76] showed that it is the redistribution of pulmonary blood flow, without a corresponding redistribution of ventilation that causes the majority of V/Q mismatch post-occlusion in pigs. However, it is not well known what happens to V/Q within the non-occluded regions, where the lung must attempt to achieve sufficient

oxygenation in a reduced functional volume of tissue. The current model does not provide a prediction of the ventilation distribution, but if we assume unchanged ventilation post-embolization [76,77], we can infer the effect of PE on V/Q. High V/Q will predominate in the occluded regions owing to minimal blood flow. Where there is a complete vascular occlusion, these distal regions will have an infinite V/Q ratio and will contribute to physiological dead space. The blood flow that would have supplied this occluded region will be redistributed to non-occluded regions, and our study has also suggested that there will be a decrease in the gravitational gradient of blood flow, which would, in turn, result in a decrease in the gradient of V/Q. This could mean that—particularly in the case of smaller occlusions or in the presence of increased ventilation and/or decreased cardiac output—the lung compensates for the reduction in lung volume by achieving a better V/Q matching in the non-occluded tissue. This point requires further analysis, with application of both computational and experimental techniques.

(*b*) *Vasoactive response to embolization*

The model predicts that occlusion to the level of segmental arteries does not increase PVR sufficiently to lead to cardiac problems. However, by simulating the gross effect of vasoactive signalling—reduced vessel elasticity or vasoconstriction—predicted PVR can be increased substantially. This result supports evidence that the release of vasoactive mediators from emboli plays an important role in whole organ response and hence disease outcome [28–30].

The model did not aim to capture the dynamics of vasoactive control—instead it analysed the impact of mechanical obstruction alone. Modelling of the dynamic constriction and dilation of vascular smooth muscle is still in its infancy. Existing models of an important vasodilator—nitric oxide (NO)—which responds to changes in shear stress (owing to flow redistribution) are reviewed by Tsoukias [78]. These are currently limited to complex models of molecular interactions, or transport at the level of a single blood vessel. Models that are able to bridge the gap between this small spatial scale and whole lung perfusion would provide additional insight into PE severity. However, it is a challenge to determine what the fundamental behaviours at the cellular level are that should be carried forward to larger spatial scales to provide an insightful and computationally achievable description of this complex process.

(*c*) *Subsegmental embolism*

Most common PE scoring systems do not consider sub-segmental emboli because they are hard to identify on CTPA and including them would certainly add precious time to the diagnostic process. As technology improves, detection of increasingly smaller emboli is becoming possible. But instead of clarifying the need for treatment, their detection raises further questions: previously undetected emboli may have remained stable or self-resolved [79–82], so should they be treated with anticoagulant therapy, which carries a risk of bleeding [83] and increases economic cost? In this study, we have assessed the potential impact of subsegmental emboli on perfusion. Our initial results suggest that subsegmental emboli located distal to a partially occluded vessel can significantly increase PVR. This provides a possible explanation for heterogeneity in PE outcome, particularly

when taken in combination with vasoactive signalling effects. It may also aid understanding of which patients may be in a higher risk category should one of their emboli fragment and create an additional occlusion.

(*d*) *Model limitations and validation*

The baseline model relies on geometrical and mathematical simplifications that are described in detail in previous studies, along with their implications on simulation results [3,13,15,42]. For example, the model does not include supernumerary arteries (SAs), which are small side branches that arise at a large branching angle from the conventional arteries (CAs) of the lung to supply the closest respiratory tissue [84] without following a matching portion of the bronchial tree. The SAs are believed to be unperfused under normal conditions [84], and their function is poorly understood. The few studies that have acknowledged the existence and distinct function of these vessels have concluded that they have unique geometry and control that limits normal perfusion but would actively divert flow under elevated pressure. For example, the origin of the SA is densely innervated [85], and is puckered into a sphincter [84] or baffle valve [86] that is suggestive of flow regulation. The effect of serotonin (a strong vasoconstrictor) in the SAs is 30 times more potent than in the CAs [87], and endogenous NO (mediates relaxation) has been shown to selectively attenuate the contractile response to serotonin in the SAs [87]. As vasoactive control mechanisms are clearly important in PE, it may be necessary to include SAs in future dynamic models of these mechanisms.

The boundary conditions (constant Q_{RV} and LAP) chosen for the current study are simplistic and not necessarily representative of the *in vivo* response to occlusion. However without quantitative definition of the relationship between Q_{RV} and LAP, setting alternate values would be arbitrary. This is a limitation of the available data, and on how this pilot study can be interpreted; however, it is not a limitation on the model itself, as the boundary conditions can readily be altered to reflect new knowledge of the Q_{RV}–LAP relationship in PE. If LAP was to increase or Q_{RV} was to decrease, then PVR and therefore PAP would—on average—be further reduced. Further simulations under these conditions (not shown here) have shown that the same trends persist, i.e. redistribution of flow to non-dependent regions, regardless of the exact levels of Q_{RV} and LAP.

The baseline model has previously been tested against perfusion measures such as PVR and flow gradients [15,42], but there is limited data available to validate the model in PE. Imaging of blood redistribution in human PE via CT will not be possible for ethical reasons; however, at the time of writing, we are conducting animal studies to obtain quantitative data on redistribution of perfusion and ventilation during inert and autologous clot preparations. These types of experiment are vital to validate the model, and confirm its predictive utility.

(*e*) *The contribution of modelling studies to understanding disease*

Modelling lung function provides an important contribution to the understanding of pulmonary health and disease. The lung is a complex organ that works dynamically and reacts rapidly to changes in posture, environment

and disease. Modelling provides a non-invasive approach to investigation of function, particularly when intervention is not possible in clinical studies owing to ill health. The type of modelling described here enables investigation of 'what if' scenarios in PE. We are able to extract information describing the physical occlusion of the vessels and can manipulate other parameters to predict what might happen under increased cardiopulmonary burden—such as additional downstream occlusions, vasoconstriction, reduced vascular compliance or a loss of capillary recruitment or perfusion area (which might occur in COPD). Predictive models such as we have developed—in hand with experiments—are powerful tools for interpreting experimental measurements and forming new testable hypotheses. Modelling also allows predictions of aspects of pulmonary function that are not readily measurable. For example, the effect of PE on perfusion in blood vessels that are not identifiable on imaging. Of course, these models must be validated against available experimental data to provide confidence in their predictions.

A further example of the utility of the modelling approach is in quantifying the significance of inter-subject variability. The models here assume that all subjects have identical distributions of arterial wall elasticity, which neglects normal variability, and any remodelling that could have occurred with age or disease. Quantifying the distribution of arterial elasticity within individual subjects is not possible. Rather than viewing this as a limitation, the model provides opportunity for studying whether this inter-subject variability is important in the context of PE and PH. While we have not performed such a study on the current patient models, it would take the form of a sensitivity analysis.

The ideal outcome of a study such as this would be to provide a definitive explanation for the range of symptoms, response to treatment and risk for secondary disease that are experienced by subjects with PE; a more realistic expectation is that it will suggest important mechanisms and patterns of vascular occlusion that merit further investigation. The long-term contribution to human health is, therefore, to pinpoint the characteristics of PE that are most worrisome, hence defining a patient that should be monitored more carefully, and conversely identifying the groups of patients for whom the risks associated with anticoagulant therapy are likely to outweigh the benefits [81,88]. This study will provide an important new approach to understand lung perfusion that will be equally applicable to studying alterations to perfusion and gas exchange in other respiratory diseases, particularly those for which PH is a component.

Use of these images and clinical data has been approved by the Northern X Regional Ethics Committee and the Auckland District Health Board Research Review Committee. Transthoracic echocardiography was used to detect RV dysfunction. This work was supported by Health Research Council of New Zealand grant number 09/143. K.S.B. was supported by an EPSRC post-doctoral fellowship at the life sciences interface.

Appendix A

The following model description summarizes the integrated model for the pulmonary circulation that was presented by Clark *et al.* [15].

(a) Extra-acinar vessels

Each extra-acinar blood vessel was defined using a one-dimensional finite element positioned within the anatomical three-dimensional lung geometry, represented by a centreline and a numeric value for its unstrained diameter (at zero transmural pressure, P_{tm}). The diameters of the left pulmonary artery (14.80 mm) and right pulmonary vein (12.97 mm) were assigned based on measurements by Huang *et al.* [89]. All other arteries and veins down to the level of the acinus were assigned diameters based on a constant rate of decrease in diameter with decreasing vessel order (the Strahler diameter ratio $R_D S$), where $R_D S$ was 1.53 in the arterial tree and 1.54 in the venous tree [15].

(b) Intra-acinar vessels

Each acinar circulatory 'unit' connects a single artery and a single vein. Within each unit, the intra-acinar vessels were explicitly represented with nine symmetric bifurcations each of arteries and veins. These intra-acinar vessels are joined at each generation by a capillary bed that covers the alveoli present at that generation, forming a 'ladder-like' structure, described previously by Clark *et al.* [13].

(c) Vessel radius as a function of pressure

Radial deformation of the extra-capillary (extra- and intra-acinar) blood vessels was related to P_{tm} by a linear relationship,

$$\frac{D}{D_0} = \alpha P_{tm} + 1, \tag{A 1}$$

where D is the strained vessel diameter and α is a compliance constant (baseline compliance, $\alpha_b = 1.50 \times 10^{-4}\,\mathrm{Pa}^{-1}$ [15]). In the larger blood vessels, $P_{tm} \approx P_b - P_e$ (where P_b is the average blood pressure across the length of the vessel and P_e is the elastic recoil pressure acting on the vessel—values were derived from a soft tissue mechanics model [41,67]). In the smallest vessels (diameter less than 200 µm), the dominant pressure acting externally to the blood vessel was assumed to be alveolar pressure (P_a), so $P_{tm} \approx P_b - P_a$ ($P_a = 0$ in this study). Capillary sheet thickness was defined using a relationship analogous to equation (A 1) [13]. Equation (A 1) is assumed valid for $P_{tm} < 32\,\mathrm{cm\,H_2O}$, beyond which the vessel is maximally extended in the radial direction.

(d) The blood flow equations

Blood flow in the extra-acinar vessels was described by the Poiseuille equation incorporating the effect of gravity acting on the blood in the direction of the vessel centreline. Thus, flow in an artery or vein was described by

$$\Delta P = \frac{128 \mu L}{\pi D^4} Q + \rho_b g L \cos \Theta, \tag{A 2}$$

where ΔP is the pressure drop along the vessel of length L, μ is the viscosity of blood in the vessel ($\mu = 3.36 \times 10^{-3}\,\mathrm{Pa\,s}$), Q is the volumetric blood flow rate, ρ_b is the blood density in the vessel ($\rho_b = 1.05 \times 10^{-6}\,\mathrm{kg\,mm^{-3}}$), g represents gravitational acceleration ($9.81\,\mathrm{m\,s^{-2}}$) and Θ is the angle that the vector along

the centreline of the blood vessel makes with the direction of gravity. The gravity vector is oriented along the craniocaudal axis (representative of the upright posture) in this study.

Gravity in the acinar arterioles and venules was neglected; therefore, flow in the arterioles and venules was described by Poiseuille's equation,

$$\Delta P = \frac{128\mu L}{\pi D^4} Q. \tag{A 3}$$

Finally, blood flow in a capillary sheet was described using the sheet flow model of Fung & Sobin [48]

$$Q = \frac{SA}{\mu_C f l_C^2} \int H^3 \, \mathrm{d}P_{\mathrm{tm}}, \tag{A 4}$$

where S is the proportion of alveolar surface area comprised capillaries ($S = 0.86$ (no units)), A is alveolar surface area ($A = 73\,\mathrm{m}^2$ – at total lung capacity (TLC)), μ_C is the apparent viscosity of blood in the capillaries ($\mu_C = 1.92 \times 10^{-3}\,\mathrm{Pa\,s}$), f is a numerical friction factor ($f = 21.6$ (no units)) and l_C is the average path length from an arteriole to a venule through the capillary network ($l_C = 1186 \times 10^{-6}\,\mathrm{m}$ at TLC). In the above equations ((A 2)–(A 4)), we solved for ΔP, and Q. D (or H) was then updated based on the pressure values and the solution was iterated until convergence was reached.

(*e*) *Capillary recruitment*

A model of capillary recruitment was incorporated into the sheet flow model. This model predicted the proportion of capillary bed perfused (p_{cap}) as a function of capillary blood pressure (P_{cap}) as follows:

$$p_{\mathrm{cap}} = 1 - F_{\mathrm{rec}} \exp\left(-\frac{P_{\mathrm{cap}}^2}{\sigma_{\mathrm{rec}}^2}\right), \tag{A 5}$$

where the constants $F_{\mathrm{rec}} = 0.65$ and $\sigma_{\mathrm{rec}} = 22.7\,\mathrm{cm\,H2O}$ (2.23 kPa) were fitted to the raw data of Godbey *et al.* [90]. Capillary surface area (A in equation (A 4)) was scaled by p_{cap} in the flow and pressure calculations.

References

1 Hoffman, E. A. *et al.* 2004 The comprehensive imaging-based analysis of the lung: a forum for team science (1). *Acad. Radiol.* **11**, 1370–1380. (doi:10.1016/j.acra.2004.09.005)

2 Tawhai, M. H., Hunter, P. J., Tschirren, J., Reinhardt, J. M., McLennan, G. & Hoffman, E. A. 2004 CT-based geometry analysis and finite element models of the human and ovine bronchial tree. *J. Appl. Physiol.* **97**, 2310–2321. (doi:10.1152/japplphysiol.00520.2004)

3 Burrowes, K. S., Hunter, P. J. & Tawhai, M. H. 2005 Anatomically-based finite element models of the human pulmonary arterial and venous trees including supernumerary vessels. *J. Appl. Physiol.* **99**, 731–738. (doi:10.1152/japplphysiol.01033.2004)

4 Lin, C.-L., Tawhai, M. H., McLennan, G. & Hoffman, E. A. 2008 Computational fluid dynamics. *IEEE Eng. Med. Biol. Mag.* **28**, 25–33.

5 Yin, Y., Choi, J., Hoffman, E. A., Tawhai, M. H. & Lin, C.-L. 2010 Simulation of pulmonary air flow with a subject-specific boundary condition. *J. Biomech.* **43**, 2159–2163. (doi:10.1016/j.jbiomech.2010.03.048)

6 Burrowes, K. S. & Tawhai, M. H. 2006 Computational predictions of pulmonary blood flow gradients: gravity versus structure. *Respir. Physiol. Neurobiol.* **154**, 515–523. (doi:10.1016/j.resp.2005.11.007)
7 Tawhai, M. H., Nash, M. P. & Hoffman, E. A. 2006 An imaging-based computational approach to model ventilation distribution and soft-tissue deformation in the ovine lung. *Acad. Radiol.* **13**, 113–120. (doi:10.1016/j.acra.2005.09.088)
8 Lin, C.-L., Tawhai, M. H., McLennan, G. & Hoffman, E. A. 2007 Characteristics of the turbulent laryngeal jet and its effect on airflow in the human intra-thoracic airways. *Respir. Physiol. Neurobiol.* **157**, 295–309. (doi:10.1016/j.resp.2007.02.006)
9 Tawhai, M. H. & Lin, C.-L. 2010 Image-based modeling of lung structure and function. *J. Magn. Reson. Imag.* **32**, 1421–1431. (doi:10.1002/jmri.22382)
10 Tawhai, M. H., Hoffman, E. A. & Lin, C.-L. 2009 The lung physiome: merging imaging-based measures with predictive computational models. *Wiley Interdiscip. Rev. Syst. Biol. Med.* **1**, 61–72. (doi:10.1002/wsbm.17)
11 Burrowes, K. S., Swan, A. J., Warren, N. J. & Tawhai, M. H. 2008 Towards a virtual lung: multi-scale, multi-physics modelling of the pulmonary system. *Phil. Trans. R. Soc. A* **366**, 3247–3263. (doi:10.1098/rsta.2008.0073)
12 World Health Organization. 2008 *World health statistics*. World Health Organization Press: Geneva, Switzerland.
13 Clark, A. R., Burrowes, K. S. & Tawhai, M. H. 2010 Contribution of serial and parallel micro-perfusion to spatial variability in pulmonary inter- and intra-acinar blood flow. *J. Appl. Physiol.* **108**, 1116–1126. (doi:10.1152/japplphysiol.01177.2009)
14 Ghaye, B., Ghuysen, A., Bruyere, P. J., D'Orio, V. & Dondelinger, R. F. 2006 Can CT pulmonary angiography allow assessment of severity and prognosis in patients presenting with pulmonary embolism? What the radiologist needs to know. *Radiographics* **26**, 23–39. (doi:10.1148/rg.261055062)
15 Clark, A. R., Tawhai, M. H., Hoffman, E. A. & Burrowes, K. S. 2011 The interdependent contributions of gravitational and structural features to distribution in a multi-scale model of the pulmonary circulation. *J. Appl. Physiol.* **110**, 943–955. (doi:10.1152/japplphysiol.00775.2010)
16 Galie, N. *et al.* 2009 Guidelines for the diagnosis and treatment of pulmonary hypertension. *Eur. Heart J.* **30**, 2493–2573. (doi:10.1093/eurheartj/ehp297)
17 Kovacs, G., Berghold, A., Scheidl, S. & Olschewski, H. 2009 Pulmonary arterial pressure during rest and exercise in healthy subjects: a systematic review. *Eur. Respir. J.* **34**, 888–894. (doi:10.1183/09031936.00145608)
18 Anderson, F. A., Wheeler, H. B., Goldberg, R. J., Hosmer, D. W., Patwardhan, N. A., Jovanovic, B., Forcier, A., & Dalen, J. E. 1991 A populations-based perspective of the hospital incidence and case-fatality rates of deep vein thrombosis and pulmonary embolism: the Worcester DVT study. *Arch. Intern. Med.* **151**, 933–938. (doi:10.1001/archinte.151.5.933)
19 Heit, J. A. 2003 Risk factors for venous thromboembolism. *Clin. Chest Med.* **24**, 1–12. (doi:10.1016/S0272-5231(02)00077-1)
20 Sox, H. S. 2006 Better care for patients with suspected pulmonary embolism (editorial). *Ann. Intern. Med.* **144**, 210–212.
21 Ryu, J. H., Olson, E. J. & Pellikka, P. A. 1998 Clinical recognition of pulmonary embolism: problem of unrecognized and asymptomatic cases. *Mayo Clin. Proc.* **73**, 873–879. (doi:10.4065/73.9.873)
22 Haunch, O., Jorgensen, L. N., Khattar, S. C., Teglbjaerg, C. S., Wahlin, A. B., Rathenborg, P. & Wille-Jørgensen, P. 1990 Fatal pulmonary embolism associated with surgery. *Acta Chir. Scand.* **156**, 747–749.
23 Karwinski, B. & Svendsen, E. 1989 Comparison of clinical and postmortem diagnosis of pulmonary embolism. *J. Clin. Pathol.* **42**, 135–139. (doi:10.1136/jcp.42.2.135)
24 Silfvast, T. 1991 Cause of death in unsuccessful prehospital resuscitation. *J. Intern. Med.* **229**, 331–335. (doi:10.1111/j.1365-2796.1991.tb00355.x)
25 Iles, S., Beckert, L., Than, M. & Town, I. 2003 Making a diagnosis of pulmonary embolism–new methods and clinical issues. *N. Z. Med. J.* **116**, U499.

26 Hull, R. D. 2006 Diagnosing pulmonary embolism with improved certainty and simplicity. *J. Am. Med. Assoc.* **295**, 213–235. (doi:10.1001/jama.295.2.213)
27 D'Alonzo, G. E. & Dantzker, D. R. 1984 Gas exchange alterations following pulmonary thromboembolism. *Clin. Chest Med.* **5**, 411–419.
28 Smulders, Y. M. 2000 Pathophysiology and treatment of haemodynamic instability in acute pulmonary embolism: the pivotal role of pulmonary vasoconstriction. *Cardiovasc. Res.* **48**, 23–33. (doi:10.1016/S0008-6363(00)00168-1)
29 Delcroix, M., Mélot, C., Lejeune, P., Leeman, M. & Naeije, R. 1990 Effects of vasodilators on gas exchange in acute canine embolic pulmonary hypertension. *Anesthesiology* **72**, 77–84. (doi:10.1097/00000542-199001000-00015)
30 Smulders, Y. M. 2001 Contribution of pulmonary vasoconstriction to haemodynamic instability after acute pulmonary embolism: implications for treatment? *The Netherlands J. Med.* **58**, 241–247. (doi:10.1016/S0300-2977(01)00117-6)
31 McIntyre, K. & Sasahara, A. 1971 Hemodynamic alterations related to extent of lung scan perfusion defect in pulmonary embolism. *J. Nucl. Med.* **4**, 166–170.
32 McIntyre, K. & Sasahara, A. 1971 The hemodynamic response to pulmonary embolism in patients without prior cardiopulmonary disease. *Am. J. Cardiol.* **28**, 288–294. (doi:10.1016/0002-9149(71)90116-0)
33 Pengo, V. *et al.* 2004 Incidence of chronic thromboembolic pulmonary hypertension after pulmonary embolism. *N. Engl. J. Med.* **350**, 2257–2264. (doi:10.1056/NEJMoa032274)
34 Tapson, V. F. & Humbert, M. 2006 Incidence and prevalence of chronic thromboembolic pulmonary hypertension: from acute to chronic pulmonary embolism. *Proc. Am. Thorac. Soc.* **3**, 564–567. (doi:10.1513/pats.200605-112LR)
35 Becattini, C., Agnelli, G., Pesavento, R., Silingardi, M., Poggio, R., Taliani, M. & Ageno, W. 2006 Incidence of chronic thromboembolic pulmonary hypertension after a first episode of pulmonary embolism. *Chest* **130**, 172–175. (doi:10.1378/chest.130.1.172)
36 Macdougall, D. A., Feliu, A. L., Boccuzzi, S. J. & Lin, J. 2006 Economic burden of deep-vein thrombosis, pulmonary embolism, and post-thrombotic syndrome. *Am. J. Health Syst. Pharm.* **63**(Suppl. 6), S5–S15. (doi:10.2146/ajhp060388)
37 Davidson, B. L. & Karmy-Jones, R. 2006 When pulmonary embolism treatment isn't working. *Chest* **129**, 839–840. (doi:10.1378/chest.129.4.839)
38 Rich, S., Levitsky, S. & Brundage, B. H. 1988 Pulmonary hypertension from chronic pulmonary thromboembolism. *Anna. Intern. Med.* **108**, 425–434.
39 Fedullo, P. F., Rubin, L. J., Kerr, K. M., Auger, W. R. & Channick, R. N. 2000 The natural history of acute and chronic thromboembolic disease: the search for the missing link. *Eur. Respir. J.* **15**, 435–437. (doi:10.1034/j.1399-3003.2000.15.01.x)
40 Huang, W., Tian, Y., Gao, J. & Yen, R. T. 1998 Comparison of theory and experiment in pulsatile flow in cat lung. *Ann. Biomed. Eng.* **26**, 812–820. (doi:10.1114/1.107)
41 Burrowes, K. S. & Tawhai, M. H. 2010 Coupling of lung tissue tethering force to fluid dynamics in the pulmonary circulation. *Int. J. Num. Method Biomed. Eng.* **26**, 862–875 (doi:10.1002/cnm.1386).
42 Burrowes, K. S., Hoffman, E. A. & Tawhai, M. H. 2009 Species-specific pulmonary arterial asymmetry determines species differences in regional pulmonary perfusion. *Ann. Biomed. Eng.* **37**, 2497–2509. (doi:10.1007/s10439-009-9802-2)
43 Li, C. W. & Cheng, H. D. 1993 A nonlinear fluid model for pulmonary blood circulation. *J. Biomech.* **26**, 653–664. (doi:10.1016/0021-9290(93)90029-E)
44 Tang, B. T., Fonte, T. A., Chan, F. P., Tsao, P. S., Feinstein, J. A. & Taylor, C. A. 2010 Three-dimensional hemodynamics in the human pulmonary arteries under resting and exercise conditions. *Ann. Biomed. Eng.* **1**, 347–358. (doi:10.1007/s10439-010-0124-1)
45 Parker, J. C., Cave, C. B., Ardell, J. L., Hamm, C. R. & Williams, S. G. 1997 Vascular tree structure affects lung blood flow heterogeneity simulated in three dimensions. *J. Appl. Physiol.* **83**, 1370–1382.
46 Glenny, R. W. & Robertson, H. T. 1991 Fractal modeling of pulmonary blood flow heterogeneity. *J. Appl. Physiol.* **70**, 1024–1030.

47 Spilker, R. L., Feinstein, J. A., Parker, D. W., Reddy, V. M. & Taylor, C. A. 2007 Morphometry-based impedance boundary conditions for patient-specific modeling of blood flow in pulmonary arteries. *Ann. Biomed. Eng.* **35**, 546–559. (doi:10.1007/s10439-006-9240-3)
48 Fung, Y. & Sobin, S. 1969 Theory of sheet flow in lung alveoli. *J. Appl. Physiol.* **26**, 472–488.
49 Dhadwal, A., Wiggs, B., Doerschuk, C. & Kamm, R. 1997 Effects of anatomic variability on blood flow and pressure gradients in the pulmonary circulation. *J. Appl. Physiol.* **83**, 1711–1720.
50 Huang, Y., Doerschuk, C. M. & Kamm, R. D. 2001 Computational modeling of RBC and neutrophil transit through the pulmonary capillaries. *J. Appl. Physiol.* **90**, 545–564. (doi:10.1063/1.1379354)
51 Burrowes, K. S., Tawhai, M. H. & Hunter, P. J. 2004 Modeling RBC and neutrophil distribution through an anatomically based pulmonary capillary network. *Ann. Biomed. Eng.* **32**, 585–595. (doi:10.1023/B:ABME.0000019178.95185.ad)
52 Popel, A. S. & Johnson, P. C. 2005 Microcirculation and hemorheology. *Annu. Rev. Fluid Mech.* **37**, 43–69. (doi:10.1146/annurev.fluid.37.042604.133933)
53 Pries, A. R., Secomb, T. W., Gaehtgens, P. & Gross, J. F. 1990 Blood flow in microvascular networks. Experiments and simulation. *Circ. Res.* **67**, 826–834.
54 Pries, A. R. & Secomb, T. W. 2000 Microcirculatory network structures and models. *Ann. Biomed. Eng.* **28**, 916–921. (doi:10.1114/1.1308495)
55 Zhou, Q., Gao, J., Huang, W. & Yen, M. 2006 Vascular impedance analysis in human pulmonary circulation. *Biomed. Sci. Instrum.* **42**, 470–475.
56 Mélot, C., Delcroix, M., Closset, J., Vanderhoeft, P., Lejeune, P., Leeman, M. & Naeije R. 1995 Starling resistor versus distensible vessel models for embolic pulmonary hypertension. *Am. J. Physiol. Heart Circ. Physiol.* **268**, H817–H27.
57 Mitzner, W. & Sylvester, J. T. 1981 Hypoxic vasoconstriction and fluid filtration in pig lungs. *J. Appl. Physiol.* **51**, 1056–1071.
58 Haworth, S. T., Linehan, J. H., Bronikowski, T. A. & Dawson, C. A. 1991 A hemodynamic model representation of the dog lung. *J. Appl. Physiol.* **70**, 15–26.
59 Zhuang, F. Y., Fung, Y. C. & Yen, R. T. 1983 Analysis of blood flow in cat's lung with detailed anatomical and elasticity data. *J. Appl. Physiol.* **55**, 1341–1348.
60 Roselli, R. J. & Parker, R. E. 1987 Venous occlusion measurement of pulmonary capillary pressure: effects of embolization. *J. Appl. Physiol.* **63**, 2340–2342.
61 Qanadli, S. D. *et al.* 2001 New CT index to quantify arterial obstruction in pulmonary embolism: comparison with angiographic index and echocardiography. *Am. J. Roentgenol.* **176**, 1415–1420.
62 Ng, C. S., Wells, A. U. & Padley, S. P. 1999 A CT sign of chronic pulmonary arterial hypertension: the ratio of main pulmonary artery to aortic diameter. *J. Thorac. Imag.* **14**, 270–278. (doi:10.1097/00005382-199910000-00007)
63 Stein, P. D. & Henry, J. W. 1997 Prevalence of acute pulmonary embolism in central and subsegmental pulmonary arteries and relation to probability interpretation of ventilation/perfusion lung scans. *Chest* **111**, 1246–1248. (doi:10.1378/chest.111.5.1246)
64 Oser, R. F., Zuckerman, D. A., Gutierrez, F. R. & Brink, J. A. 1996 Anatomic distribution of pulmonary emboli at pulmonary angiography: implications for cross-sectional imaging. *Cardiovasc. Radiol.* **199**, 31–35.
65 Pryce, D. M. & Heard, B. E. 1954 The distribution of experimental pulmonary emboli in the rabbit. *J. Pathol. Bacteriol.* **71**, 15–25. (doi:10.1002/path.1700710104)
66 Fung, Y. C. & Sobin, S. S. 1972 Pulmonary alveolar blood flow. *Circ. Res.* **30**, 470–490.
67 Tawhai, M., Nash, N., Lin, C.-L. & Hoffman, E. 2009 Supine and prone differences in regional lung density and pleural pressure gradients in the human lung with constant shape. *J. Appl. Physiol.* **107**, 912–920. (doi:10.1152/japplphysiol.00324.2009)
68 Hopkins, S. R., Henderson, A. C., Levin, D. L., Yamada, K., Arai, T., Buxton, R. B. & Prisk, G. K. 2007 Vertical gradients in regional lung density and perfusion in the supine human lung: the Slinky effect. *J. Appl. Physiol.* **103**, 240–248. (doi:10.1152/japplphysiol.01289.2006)
69 West, J. B., Dollery, C. T. & Naimark, A. 1964 Distribution of blood flow in isolated lung; relation to vascular and alveolar pressures. *J. Appl. Physiol.* **19**, 713–724.
70 Glenny, R. W., Bernard, S., Robertson, H. T. & Hlastala, M. P. 1999 Gravity is an important but secondary determinant of regional pulmonary blood flow in upright primates. *J. Appl. Physiol.* **86**, 623–632.

71 Glenny, R. W., Lamm, W. J. E., Albert, R. K. & Robertson, H. T. 1991 Gravity is a minor determinant of pulmonary blood flow distribution. *J. Appl. Physiol.* **71**, 620–629.
72 Mélot, C. & Naeije, R. 2000 Pulmonary vascular diseases. In *Pulmonary and peripheral gas exchange in health and disease* (eds J. Roca, R. Rodriguez-Roisin & P. D. Wagner). New York, NY: Marcel Dekker.
73 Dantzker, D. R. & Bower, J. S. 1982 Alterations in gas exchange following pulmonary thromboembolism. *Chest* **81**, 495–501. (doi:10.1378/chest.81.4.495)
74 Mure, M., Domino, K., Lindahl, S., Hlastala, M., Altemeier, W. & Glenny, R. 2000 Regional ventilation-perfusion distribution is more uniform in the prone position. *J. Appl. Physiol.* **88**, 1076–1083.
75 Petersson, J. *et al.* 2009 Regional lung blood flow and ventilation in upright humans studied with quantitative SPECT. *Respir. Physiol. Neurobiol.* **166**, 54–60. (doi:10.1016/j.resp.2009.01.008)
76 Altemeier, W., Robertson, H., McKinney, S. & Glenny, R. 1998 Pulmonary embolization causes hypoxemia by redistributing regional blood flow without changing ventilation. *J. Appl. Physiol.* **85**, 2337–2343.
77 Tsang, J., Frazer, D. & Hlastala, M. P. 2000 Ventilation heterogeneity does not change following pulmonary microembolism. *J. Appl. Physiol.* **88**, 705–712. (doi:10.1063/1.373725)
78 Tsoukias, N. M. 2008 Nitric oxide bioavailability in the microcirculation: insights from mathematical models. *Microcirculation* **15**, 813–834. (doi:10.1080/10739680802010070)
79 Perrier, A., Bounameaux, H. 2006 Accuracy or outcome in suspected pulmonary embolism. *N. Engl. J. Med.* **354**, 2383–2385. (doi:10.1056/NEJMe068076)
80 Stein, P. D. *et al.* 2006 Multidetector computed tomography for acute pulmonary embolism. *N. Engl. J. Med.* **354**, 2317–2327. (doi:10.1056/NEJMoa052367)
81 Egermayer, P. & Town, G. I. 1997 The clinical significance of pulmonary embolism: uncertainties and implications for treatment—a debate. *J. Intern. Med.* **241**, 5–10. (doi:10.1046/j.1365-2796.1997.74880000.x)
82 Le Gal, G., Righini, M., Parent, F., van Strijen, M. & Couturaud, F. 2006 Diagnosis and management of subsegmental pulmonary embolism. *J. Thromb. Haemostatis* **4**, 724–731. (doi:10.1111/j.1538-7836.2006.01819.x)
83 Egermayer, P., Inder, A. & Town, G. I. 2001 The use of warfarin in Christchurch for the treatment of venous thromboembolism. *N. Z. Med. J.* **114**, 336–338.
84 Elliot, F. M. & Reid, L. 1965 Some new facts about the pulmonary artery and its branching pattern. *Clin. Radiol.* **16**, 193–198. (doi:10.1016/S0009-9260(65)80042-3)
85 Filenz, M. 1970 Innervation of pulmonary and bronchial blood vessels of the dog. *J. Anat.* **106**, 449–461.
86 Bunton, D. C., Fisher, A., Shaw, A. M., MacDonald, A., Montgomory, I. & McGrath, J. C. 1996 Musculo-elastic structure at origin of pulmonary supernumerary artery resembles a baffle valve 119. *Br. J. Pharmacol.* **119**, 323P.
87 Bunton, D., MacDonald, A., Brown, T., Tracey, A., McGrath, J. & Shaw, A. 2000 5-Hydroxytryptamine- and U46619-mediated vasoconstriction in bovine pulmonary conventional and supernumerary arteries: effect of endogenous nitric oxide. *Clin. Sci.* **98**, 81–89. (doi:10.1042/CS19990115)
88 Dalen, J. E. 2002 Pulmonary embolism: what have we learned since Virchow? *Chest* **122**, 1440–1456. (doi:10.1378/chest.122.4.1440)
89 Huang, W., Yen, R. T., McLaurine, M. & Bledsoe, G. 1996 Morphometry of the human pulmonary vasculature. *J. Appl. Physiol.* **81**, 2123–2133.
90 Godbey, P. S., Graham, J. A., Presson Jr, R. G., Wagner Jr, W. W. & Lloyd, Jr, T. C. 1995 Effect of capillary pressure and lung distension on capillary recruitment. *J. Appl. Physiol.* **79**, 1142–1147.